

Thermal Decomposition Mechanisms of 4-Nitroimidazole(4NI)  
Using Time Resolved Pulsed Photoacoustic Technique at 532 nm

دراسة التحلل الحراري لل-4-نيتروائيمييدازول باستخدام التقنية الضوء-صوتية  
المعتمدة على التحلل النبضي الزمني عند طول موجي 532 نانومتر

**Dr. Fahem Yehya Ahmed Bajash<sup>(1)</sup>**

---

(1) Assistance professor in the department of Physic, Faculty of Education & Sciences ,  
Albaydha University, Albaydha , Yemen.

fahembajash@gmail.com



## Thermal Decomposition Mechanisms of 4-Nitroimidazole(4NI) Using Time Resolved Pulsed Photoacoustic Technique at 532 nm

### ABSTRACT

The paper reports a novel approach based on time resolved pulsed Photo acoustic (PA) and TG-DTA techniques to study the thermal decomposition mechanisms of **4-Nitroimidazole(4NI)** at 532 nm. The study is based on the detection of NO<sub>2</sub> released by these samples under different thermal zones. The second harmonic i.e.  $\lambda = 532$  nm pulses of 7 ns width obtained from Q-switched Nd: YAG laser is employed to record the time and temperature dependent PA spectrum in a specially designed photoacoustic system. The

multistep thermal decomposition mechanisms in terms of new NO<sub>2</sub> thermal windows which is a part of N-N bond and concerted ring breaking mechanism of HEMs, is reported. The combination of PA and TG-DTA results open a new channel to understand the generation mechanism of free NO<sub>2</sub> at different temperatures and leads to develop a new tool to scale the HEMs efficiency as a fuel

**Keywords:** Photo acoustic; temperature, Nd: YAG Laser; HEMs

### الملخص

أنظمة ضوء-صوتية خاصة. تم قياس أطيف ثاني أكسيد النيتروجين المنحلة جزئياً من تفكك كل من روابط النيتروجين-النيتروجين و بقية حلقات المواد ذات الطاقة العالية خلال مراحل متعددة للتحلل الحراري. إن مقارنة نتائج التحلل الحراري باستخدام الطريقة الضوء-صوتية مع نتائج طريقة التحلل الحراري الوزني تساعدنا في فهم أكثر لميكانيكية تفكك مجموعات ثاني أكسيد النيتروجين عند درجات حرارة مختلفة.

البحث يتضمن دراسة التحلل الحراري لـ 4- نيتروايميدازول باستخدام التقنية الضوء-صوتية المعتمدة على التحلل النبضي الزمني عند طول موجي 532 نانومتر. الدراسة تعتمد على قياس ثاني أكسيد النيتروجين المنحلة من المركب خلال مراحل مختلفة للتحلل الحراري. تم استخدام الليزر النبضي الياج- ناديميوم (نوع مفتاح كيو) بطول موجي 532 نانومتر و عرض النبضة 7 نانوثانية لقياس الأطيف الصوتية في النطاق الزمني والحراري داخل

## 1. Introduction:

Generally, the molecules having nitro groups are conventionally assigned as energetic materials. The present global trend is to develop an eco-friendly high energy materials which should possess high detonation performance in combination with good thermal stability and insensitive towards shock and friction and used as efficient rocket fuel. The existing benchmark secondary HEMs such as 1,3,5 trinitro per hydro 1,3,5 – triazine (RDX) , RDX, TNT, HMX , PETN etc. follows different mechanism to release energy which includes N-N bonds and concentrated ring breaking and formation of nitrogen oxide etc. Imidazole is a heterocyclic compound of five-member di-unsaturated ring structure composed of three carbon atoms and two nitrogen atoms at non adjacent positions. Imidazole and Its derivatives exposed for research by many groups due to their important role in medical applications. They are widely used as intermediates in synthesis of organic target compounds including pharmaceuticals, agrochemicals, epoxy curing agents, dyes, photographic chemicals, corrosion inhibitors, adhesives and plastic modifiers. Moreover, Nitroimidazoles group has spectrum of activity against Gram-positive and Gram-negative bacteria and hypoxic tumours. However, due to their favorable physical parameters and high detonation velocity they are also treated as high energy density materials which have attracted renewed attention of propellant experts [( Venkatesh,203- Yehya,2013 – Larina,2009 – Phukan,2011)].

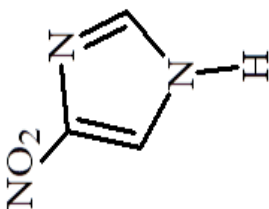


*Figure-1: Structure of 4-Nitroimidazole*

The thermal decomposition mechanism of HEMs is still one of the challenging tasks. Several groups have extensively developed theoretical approach to understand the molecular dynamics (MD) and given the mechanism of bond breaking in several steps [3-6]. They have reported that thermal decomposition in HEMs followed by three most important channels: **(a) the first one** is uni-molecular decomposition which produces HONO, **(b) the second path** follows the hemolytic cleavage of an N-N bond which release of NO<sub>2</sub>, and **(c) third path** follows the concerted ring

fission. In all these cases the  $\text{NO}_2$  was found as a one of the principal byproduct. Moreover, the prediction has been made at very high temperature i.e. above  $1200^\circ\text{C}$ . There are some experimental reports on thermal decomposition mechanism of HEMs samples are also available which confirms the release of  $\text{NO}_2$  above their melting point i.e. more than  $200^\circ\text{C}$ . The percentage amount of released  $\text{NO}_2$  which is also known as fragmented mass varies with the detonation velocity. It is important to note that the N-N bond breaking to form  $\text{NO}_2$  is the predominant part of the chemical reaction though the energy barrier for the HONO is as similar to the  $\text{NO}_2$ . But  $\text{NO}_2$  formation mechanism leads to increase the entropy (less free energy) while HONO elimination has a low entropy and high free energy. The important transitions of the defragmented molecules which produce by the thermal decomposition of HEMs are shown in Table-1(a) and the band energies of the weakest band in HEMs are shown in Table-1(b) [(Gutowski,2007- Ren,2011- Li,2010- Agrawal,2010- Schubert,2006 - Akhavan,2007)]

**Table-1(a): Thermal decomposition pathways in nitramine propellants.**

No.	Molecule(atom s radiant)	Transition	Laser wavelength	Emission wavelength
1	NO	$A^2\Sigma^-X^2\pi$	226	248
2	OH	$A^2\Sigma^+X^2\pi$	281	312
3	NH	$A^3\pi-X^2\Sigma^-$	336	336
4	CH	$B^2\Sigma^-X^2\pi$	387	390
5	CN	$B^2\Sigma-X^2\Sigma$	388	421
6	$\text{NO}_2$	$A^3B_1-X^2A_1$	400	440
7	OH	$A^2\Delta-X^2\pi$	413	430

**Table-1(b): Band energies of weakest band**

No.	Compound	Trigger linkage	Band energy KJ/mol	Kcal/mol	Activation energy KJ/mol	Kcal/mol
1	Nitroarene	C—NO <sub>2</sub>	305	73	293	70
2	Nitramine	N—NO <sub>2</sub>	163	39	196	47
3	Nitrate Ester	CO—NO <sub>2</sub>	222	53	167	40
4	Peroxide	CO—OC	142	34	146	35

The photoacoustic technique offers the advantages of high sensitivity, selectivity, compact setup and fast time-response, and is widely recognized for its excellent performance in trace gas measurement from ppm to ppb level[17-36]. Several groups have reported the photoacoustic studies on NO<sub>2</sub> using second harmonic of pulsed Nd: YAG laser, however, these studies are restricted to pure NO<sub>2</sub> gas (Sigrist,1994,2001 –Yehya,2011-2020, Naseem,2020,- Thöny,1995-Miklós,2001- Harren,2000, - Rao-205)

Since NO<sub>2</sub> has an absorption band in the UV-Visible region (300–600 nm), therefore, the 532 and 266 nm radiations generated by second and fourth harmonic of Nd: YAG laser with a pulse width of 7 ns and repetition rate of 10 Hz can be treated as one of the ideal source for time resolved spectroscopy of nitro compounds. Moreover, the life time of the radiative vibrational levels is long compared to the life time of the collisional deactivation. Therefore, the absorbed energy is completely released in the form of heat from the sample. A few pulsed lasers based photoacoustic studies on pure NO<sub>2</sub> gas are available (Yehya,2011-2020)

The paper discusses the new multidimensional aspects of an improvised form of an existing PA technique. It is employed to study the thermal decomposition mechanism of 4-Nitroimidazole sample. We have recorded the acoustic finger prints in time and frequency domain. The study also confirms the multistep bond breaking thermal decomposition mechanisms of HEMs. Moreover, the role of oxidation reaction is the part of formation of NO<sub>2</sub> at higher temperature. Finally, our findings combined with TG-DTA analyses provides a new tool to identify some of the important features of the HEMs such as thermal gaseous bi-products, and relationship between residual amount of the samples and the efficiency of the fuel for the first time.

## 2. Experimental Details:

The second harmonic of Q-switched Nd: YAG laser (Model Spit, Germany) is used to excite the thermally released  $\text{NO}_2$  molecules in a specially designed photoacoustic system which has a stainless made cell of internal diameter of 15 mm, length of 7.5 cm (as shown in fig-3). The samples are heated in a round bottom flask using temperature controlled oven. A needle valve is used to control the flow rate of vapor through inlet. The photoacoustic signal (PA signal) is detected by pre-polarized microphones of 50mV/Pa (BSWA, China).



*Figure-2: Schematic layout of photoacoustic experiment.*

The microphone is placed in the center of the cell. The output signal of the microphone has been fed to the preamplifier which is coupled to the 200 MHz Oscilloscope (Tektronix, U.S.A.). The USB/GPIB interfacing is used for data acquisition through Boxcar integrator (Stanford Instruments Inc., USA). Schematic layout of photoacoustic experiment is shown in Figure 1. The sample vapors are collected from solid sample in a specially designed heating system between 23 to 350°C.



*Figure-2 : PA Cell Dimension: Length= 7.5cm & Radius =1.4cm*

The special care is taken to avoid the damage of the microphone diaphragm. A special type of needle valve is used to control the inlet vapor. The collected vapor is sent into the PA cell which is irradiated by 532 nm laser beam. The generated PA signal is recorded at the desired value of incident energy, temperature and pressure.

Thermal gravimetric-differential thermal analysis (TG-DTA) is carried out using a TA instrument (Model No. Q600 DT). The ~ 1.2 mg sample is taken in alumina crucible and heated from 25 to 350 °C for the solid samples under nitrogen environment (flow rate of 100 cm<sup>3</sup>/min) as the purge and protective gas. The reference is an empty alumina crucible. Non-isothermal TGA runs were conducted from 25 to 350 °C at heating rate of the order of 10<sup>0</sup>C/min.

**3. Results and Discussions:** This part of the paper is divided into four sub sections, Section –I deal with the PA spectrum of sample. while, section –II deals with the thermal decomposition mechanism of sample based on PA technique and TG-DTA. Section -III comprises the effect of input laser energy and generated PA signals. The last section –IV deals with the combination of PA &TG-DTA results

### 3.5 Simulation part of theoretical calculated modes inside resonance cavities :

In this section we have calculate the longitudinal , radial and azimuthal resonance frequencies inside the resonance cavities as listed in table-2

*Table-2: Calculated longitudinal , radial and azimuthal modes*

	1785	3570	5360	7150
Longitudinal Modes (Hz)	8930	10720	12500	14300
	16080	17870	19650	21440
	4900	8142	11200	14175
Pure Azimuthal m=2:5	10215	14210	17880	21367
Azimuthal Modes+1 <sup>st</sup> radial	10215	18702.5	27100	35500
Pure Radial Modes				

The individual and complex longitudinal , radial and azimuthal for PA cell have been simulated and presented in figure-3. The upper row is divided to three parts: first part represents the first four pure azimuthal modes. Since, 1<sup>st</sup> azimuthal mode (Az(00)=0) the pure azimuthal modes is started from second mode up to 15kHz (i.e. Az(10), Az(20), Az(30) and Az(40)). Second part in the first row represents the first four azimuthal modes mixed with first radial mode (i.e Az(01), Az(11), Az(21) and Az(31)) up to 25kHz while third part represents the first three pure radial modes (Ra(10),Ra(20) and Ra(30) up to 40kHz. Of course, first mode in

second part (Az(01))=first mode in third part (Ra(10)). The second row represents the longitudinal modes up to 25kHz while third row represents the complex modes (Lo=40,Az=4 &Ra=4)

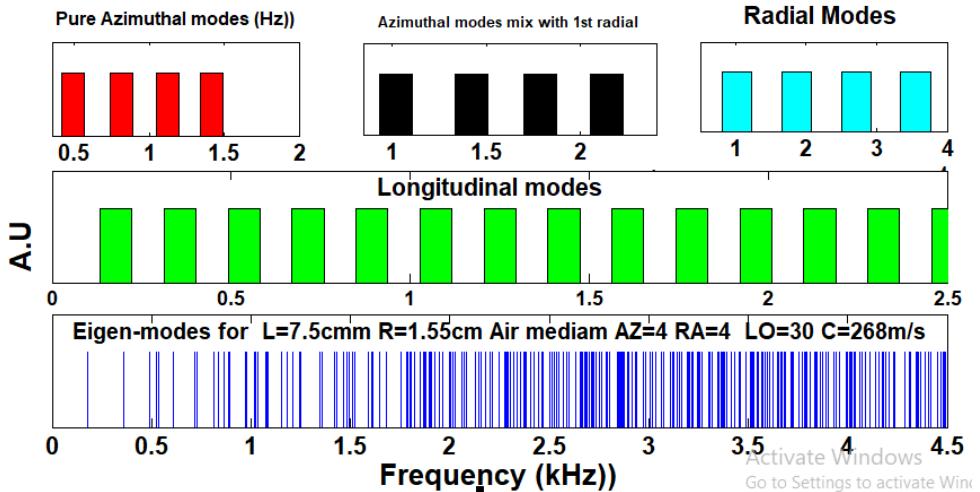


Figure-3: Simulation of resonance modes

### 3.1 PA spectra of samples

Fig-4 shows the PA signal in time domain and frequency domain using Fast Fourier transform FFT. The PA spectrum shows the clustering effect as a reflection part of the 4NI spectrum. The excited acoustic modes show that all type of modes can be excited in different conditions for the same molecules. The figure shows that the longitudinal modes are excited and dominating over radial and azimuthal modes. It shows there are appearing as two longitudinal acoustic modes which located at 1750Hz & 4700, 5800Hz, respectively. In addition, 10900, 12400, 13300, 14250, 15700 & 17600 the third radial mode is located at 27800Hz. The figure shows clearly the domination of longitudinal modes over radial and azimuthal modes. There is a small shift in the value of recorded frequency from the calculated one which is attributed to the variation of temperature. However, the other modes show different interesting features which vary from sample to sample.

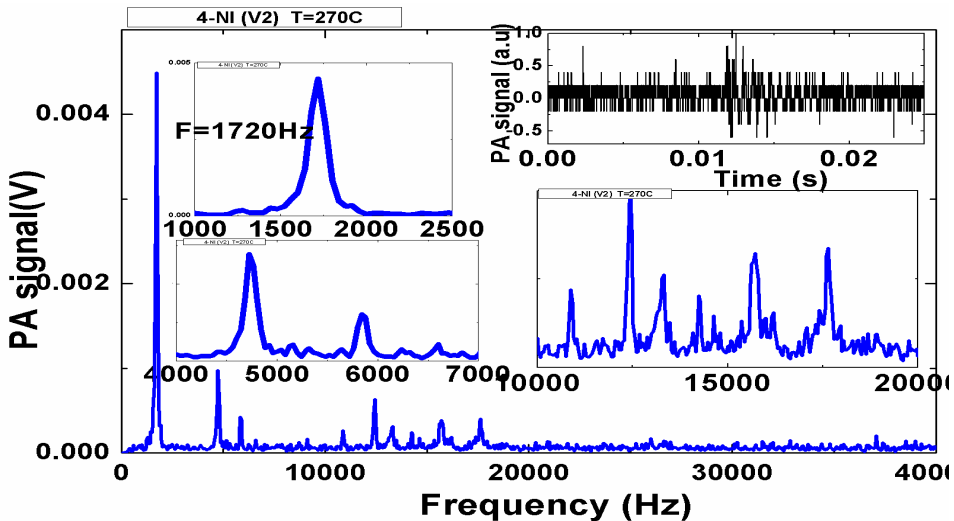
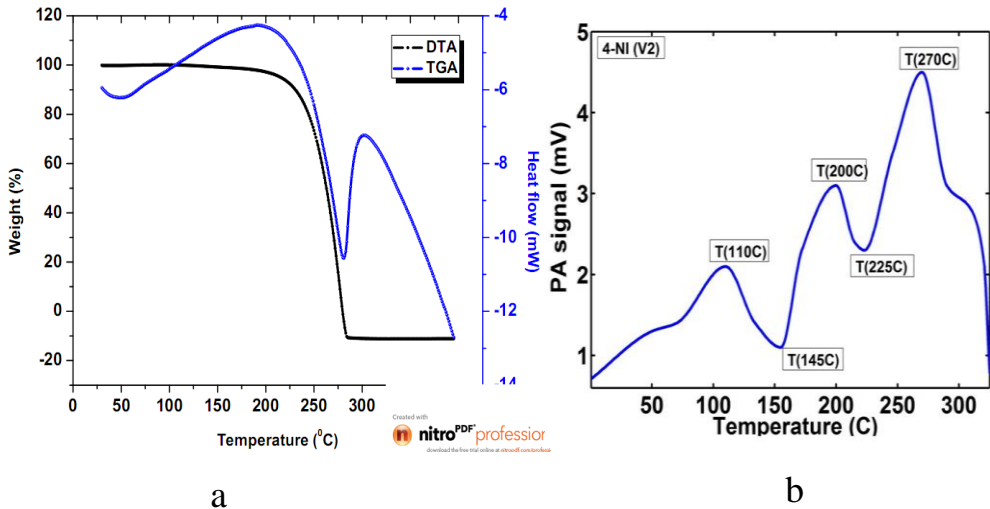


Figure-4: Eigen modes of PA cell and PA spectrum of 4NI

In the present study, the enhancement in photoacoustic (PA) signal is inferred due to increase in the number of released  $\text{NO}_2$  from the parent molecule. In case of  $\text{NO}_2$ , there is a strong coupling between the high vibrational levels of  $X^2A_1$  ground state and  $^2B_2$  or  $^2B_1$ . Consequently, the entire stored optical energy contributes towards the heating of the sample. Therefore,  $\text{NO}_2$  is excited to the  $^2B_2$  state due to absorption of 532nm which transfer its excitation energy to photo acoustic signal by V-T and V-V relaxations of  $\text{NO}_2$  through collisions with Air molecules.

### 3.2.3 Thermal decomposition study of 4NI

Fig-5(a) shows the temperature effect on the PA in which different distinguished temperature zones represent the thermal decomposition mechanism of 4NI under the influence of laser radiation. It shows that the recording signature of  $\text{NO}_2$  starts coming in multiple-steps.

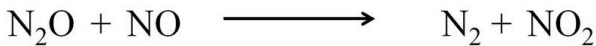
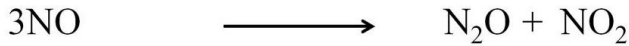
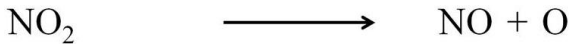


**Figure 5: (a) TG-DTA curve of 4NI (b) Temperature effect on PA signal of 4NI**

Fig-5 (b) represent TG-DTA curves. It shows that , 4NI has no weight loss observed up to 303 °C (D.P) which represent the good thermal stability of the sample. However, the maximum weight loss of the sample starts around 195 °C to 303 °C. with most rapid weight loss at 230 °C. Ravi..et al shown that, the activation energy required for the decomposition of 4-nitroimidazole according to the Friedman and the Flynn–Wall–Ozawa methods are 120 kJ mol<sup>-1</sup> and 114.7 kJ mol<sup>-1</sup>, respectively[1]. They introduce a scheme which represent the decomposition pathways of 4-nitroimidazole. The splitting of C-NO<sub>2</sub> bonds are the starting decomposition step followed by production of NO<sub>2</sub> destroyed the un-decomposed 4NI instantaneously. Finally, other bands of 1,3-diazole ring such C=N, C=C, C-H and N-H bonds were broken concurrently.[1,32]. However, The NO<sub>2</sub> and NO elimination were found to be the major decomposition production in this decomposition process. [1]

The intensity of PA signal varies with temperature such as strong peaks at 110, 200 & 270 °C, respectively. Keeping in view of safety aspects of the experiment we have restricted the temperature limit up to 340 °C. However, there is drastically increase of PA signal at third temperature peak. This process may be expressed as following: when the temperature is around 110 °C, the compound at least release one NO<sub>2</sub> group in little amount which absorbs the incident laser beam and generate PA signal then at 200 °C which is the melting point of the sample. More NO<sub>2</sub> group are

released and generating good PA signal. Now 270 °C is treated as a critical temperature (also shown in fig-3(b)). This temperature is responsible for complete defragmentation of C-NO<sub>2</sub> as well as the point of commencement of the ring breaking mechanism. The entire process produces a new batch of fresh NO<sub>2</sub> which is resulted from the oxidation of the defragmented nitrogen released by broken ring. The produced huge amount of NO<sub>2</sub> is recorded in terms of strong PA signal. The different chemical reactions involved in this process are given by the following equation [33]:



### 3.3 PA signal dependence on input laser energy:

In PA technique, signal shows two distinct cases with respect to laser intensity. The first one, at low laser beam intensity, where the PA signal is proportional to density of the gas squared,  $(t/t_c)^2$  ( $t$  and  $t_c$  are the total de-excitation life time and collisional life time) and varies linearly with the laser beam intensity ( $I_0$ ). The second case at high laser intensity, the PA signal varies with  $I_0^{-1}$  and here the absorption saturation occurs [34, 35].

Fig-6 shows the energy effect on the PA signal at different incident laser energy for strongest resonance modes .

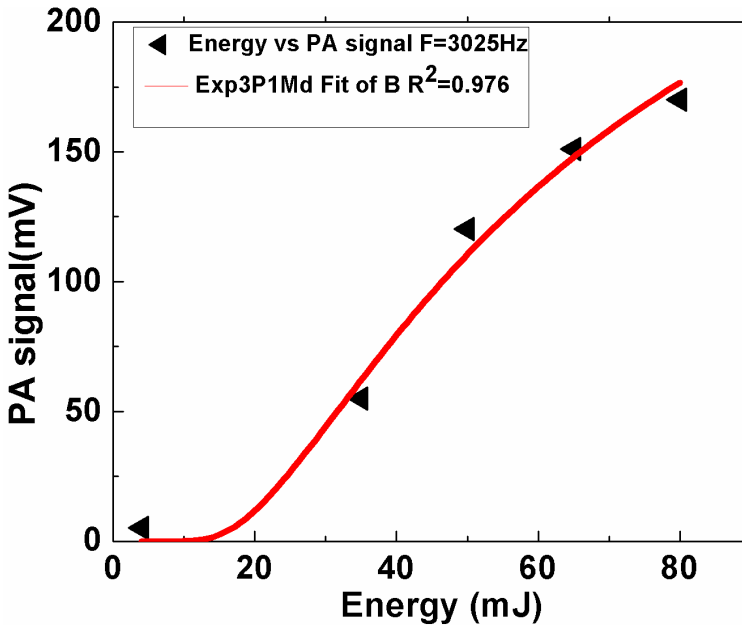


Figure 5: Energy study of (a) Sample 03

The variation found in good agreement with exponential equation:

$$y = \exp(a+b/(x+c))$$

$$\text{where } a=5.89 \pm 0.5 \quad b=-54.696 \pm 54.55 \quad c= -4 \pm 23.3$$

However, the PA signal is initially increasing slowly with input laser energy then maintains linear growth up to laser energy less than 60 mJ.

However, beyond this point the PA signal shows some sort of saturation.

### 3.4 The comparative study between PAS & TG-DTA techniques

The combined results obtained from Photoacoustic and TG-DTA techniques open a new channel of research to scale the efficiency of both techniques in thermal analyses. Table-4 shows some important information related to 4NI sample. TG-DTA shows only two important points: 198 °C which representing the beginning of weigh losses or melting point while 280 °C that representing the total decomposition/ Detonation point (D. P) . But in PA curve there are three important points : 110 °C , 200 °C & 270 °C which represents the first release of NO<sub>2</sub> (small NO<sub>2</sub> window), second releasing point of NO<sub>2</sub> (M.P) & third releasing point of NO<sub>2</sub> (D.P). it's very clear the preferred of PAS technique over TG-DTA technique. Of course theory of PA method required more development to be applicable in activation energy and other important factors.

**Table-4: some important information related to 4NI sample.**

Sample	Thermal stability T(°C)		DTA		Highest PA signal achieved at T (°C)
	From weight loss curves	From PA signal curves	T <sub>m</sub> (°C)	T <sub>d</sub> (°C)	
4NI	198	110	200	270 280	300

**Quality-Factor of the resonance cell**

One of the main factors that measure the goodness of PA cavity is the quality factor. The interesting feature of q-factor is the ability to calibrate the PA system according to value and type of the excited resonance mode. Value of quality factor reflects the quality or efficiency of the photo acoustic system at all. It shows the effecting of incident laser energy, temperature, acquisition time and sample pressure on the excited mode quality. Physically, Quality factor defined as the ratio of the accumulated energy of resonance mode in one cycle to the energy lost over one cycle. It can be written mathematically as follows:

$$Q = \frac{2\pi \text{ accumulated energy}}{\text{energy lost over one period}} = \frac{f_0}{\Delta f}$$

Where  $f_0$  and  $\Delta f$  are the resonance frequency and the full width at half maximum of the resonance profile (FWHM). Fig-6(a) shows the Lorentz fitting of the highest excited mode in Different temperature while F-g-6(b) shows the variation of Q-factor and central frequency with different values of temperature. The calculations are listed in table -5.

**Table-4 Q-factor and central frequencies with Temperature**

<b>Frequency(Hz)</b>	<b>1 723</b>	<b>1710</b>	<b>1702</b>	<b>1715</b>
<b>Temperature(°C)</b>	<b>70</b>	<b>110</b>	<b>220</b>	<b>270</b>
<b>Q-Factor</b>	<b>15</b>	<b>19</b>	<b>18</b>	<b>15</b>

Table -4 & F-g-6(b) show the invers behavior between the central resonance frequencies and quality factor. However, it's very clear that, the quality factor has a minimum values with low and high temperature. That means the efficiency of PA cell is increasing with temperature upto some value then reducing dramatically.

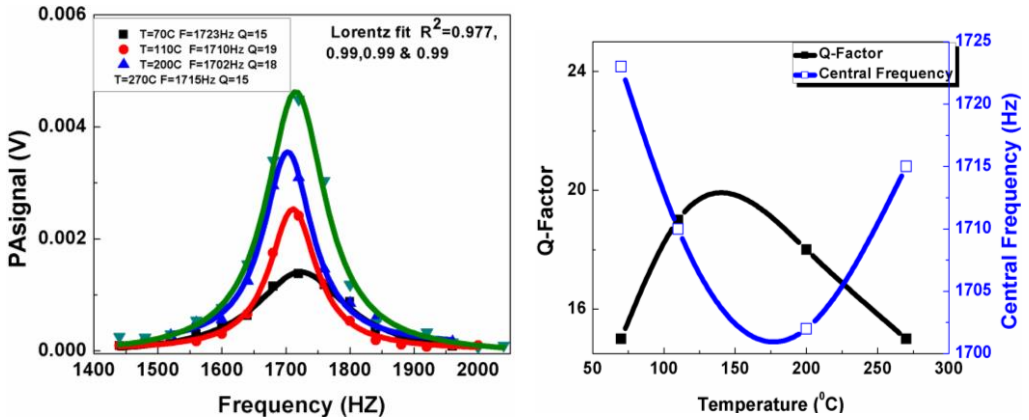


Figure-6: (a) Q-factor and (b) central frequencies with Temperature

#### 4 Conclusions:

We have successfully recorded the time resolved temperature dependent PA spectra of 4NI. This is based on the release of  $\text{NO}_2$  molecules by these solid samples under controlled state of thermal decomposition. Also, we have shown the acoustic finger spectrum of given samples. In addition, the thermal data obtained from PA and TG-DTA techniques are extended to understand the thermal decomposition mechanism of 4NI. Also, these results help to develop a new tool to scale the HEMs efficiency as a fuel for the first time. Our experimental finding confirms the presence of small thermal windows which is slightly above the room temperature. Moreover, the obtained results also confirm that the thermal decomposition mechanism for the sample follow multistep decomposition process along with release of free  $\text{NO}_2$ . It is also to be noted that the generation of  $\text{NO}_2$  group at higher temperature is only due to the oxidation reaction and observed for the samples having nitrogen in their ring structure.

#### 5. Acknowledgements

We gratefully acknowledge the Professor A. K. Chaudhary, (ACRHEM, University of Hyderabad and Department of Science and Technology (SERC Project, No: SR/S2/LOP-13/03) and Defense Research Development Organization, India for the financial support.

## 6. References

Agrawal J. P., High Energy Materials: Propellants, Explosive, Pyrotechnics. (WILEY-VCH Verlag GmbH & Co. KGaA, Weinheim -2010)

Akhavan, J. The Chemistry of Explosives (Royal society of Chemistry (RSC) - Paperbacks- UK-2005)

Gutowski K. E., Rogers R. D., Dixon D. A. , Accurate Thermochemical Properties for Energetic Materials Applications. II. Heats of Formation of Imidazolium-, 1,2,4-Triazolium, and Tetrazolium Based Energetic Salts from Isodesmic and Lattice Energy Calculations, J. Phys. Chem. B, 111(2007) 4788-4800.

Harren F. J. M. , .. et al “Photoacoustic Spectroscopy in Trace Gas Monitoring,” *Encycl. Anal. Chem.*, (2000) 2203–2226.

Larina L., Lopyrev L. ,”Nitroazoles: Synthesis, Structure and Applications”; Springer: New York, (2009).

Li, X. H.; Zhang, R. Z.; Zhang, X. Z. Computational Study of Imidazole Derivative as High Energetic Materials. *J. Hazard. Mater.*, 183(2010) 622-631

Miklós A., Hess P. , and Bozóki Z., “Application of acoustic resonators in photoacoustic trace gas analysis and metrology,” *Rev. Sci. Instrum.*, vol. 72 (4) (2001) 1937–1955.

Naseem Al-Mudfferi & Yehya F. “Simulation of photo acoustic waves based eigen value and eigen function in different geometrical resonance cell” *Al-Baydha University Journal* 2(2)(2020) 67-76.

Phukan K., Devi N., N. Greener and Versatile Synthesis of Bioactive 2-Nitroimidazoles using Microwave Irradiation. *J. Chem. Pharm. Res.* 3(2011)1037-1044.

Rao K. S. , Chaudhary A. K., Yehya F. & Kumar A. S. “Study of acoustic fingerprinting of nitromethane and some triazole derivatives using UV 266 nm pulsed photoacoustic pyrolysis technique,” *Spectrochimica Acta Part A: Molecular and Biomolecular Spectroscopy* 147 (2015) 316–323

Ren Y., Li M., Yang J., Peng J., & Gu Y., An Alternative to Nitromethane as Solvent: The Promoting Influence of Nitro-Functionalized Imidazolium Salts for Synthesis and Catalysis, *Adv. Synth. Catal.* 353 (2011) 3473–3484

Schubert H. , Kuznetsov A. , (ENato Security through Science Series B: Detection and Disposal of Improvised Explosives. (Springer-2006)

Sigrist M. W., et al “Environmental Spectroscopy Applications of Photoacoustic,” *Anal. Chem.*, 17(2001) 511–514.

Sigrist W.M. , *Air Monitoring by Spectroscopic Techniques*, New York: John Wiley and Sons(1994) .

Slezak V., Santiago G. and Peuriot A. L. , “Photoacoustic detection of NO<sub>2</sub> traces with CW and pulsed green lasers,” *Opt. Lasers Eng.*, 40, no. 1–2 (2003) 33–41.

Thöny A., and Sigrist M. W. , “New developments in CO<sub>2</sub>-laser photoacoustic monitoring of trace gases,” *Infrared Phys. Technol.*, 36 (2) (1995) 585–615.

Urbanski T., *Chemistry and Technology of Explosives*, (Pergamon Press , Oxford, UK -1984 )

Venkatesh M., Ravi Pasupala, and Tewari Surya P “Isoconversional Kinetic Analysis of Decomposition of Nitroimidazoles: Friedman Method vs. Flynn-Wall-Ozawa Method” *J. Phys. Chem. A* 12 (2013)

Yehya F. & Chaudhary A. K. "Low Limit Detection of NO<sub>2</sub> by Longitudinal Mode Selection in a Photoacoustic Resonant System” *Pramana*, 81 (3), 535 (2013)

Yehya F. & Chaudhary A. K. “A novel investigation of the thermal decomposition mechanism of (MTNI) and (KNO<sub>2</sub>) using time resolved pulsed photoacoustic technique” *Sensors and actuators B: Chemical*, 178 (2013) 324

Yehya F. & Chaudhary A. K. “Study of damping, saturation and surface losses on low level detection of NO<sub>2</sub> using time resolved pulsed photo acoustic technique,” *Opt. Commun.*, vol. 312, no. 2(2014) 16–22

Yehya F. & Chaudhary A. K. “Thermal decomposition study of Nitropyrazoles based on time-resolved pulsed photoacoustic spectroscopy” Appl. Phys. B: Laser and Optics , 110, 15 (2013)

Yehya F. & Chaudhary A. K. “Time resolved high frequency spectrum of Br<sub>2</sub> molecules using pulsed photoacoustic technique.,” Spectrochim. Acta. A. Mol. Biomol. Spectrosc., vol. 115(2013) 544–51.

Yehya F. & Chaudhary A. K. “Time Resolved Time Dependent Photo-Acoustic Spectroscopy of NO<sub>2</sub> in a High Frequency Multi -Resonant Cavity“ Appl. Phys. B: Laser and Optics, 106 (2012) 953

Yehya F. & Chaudhary A. K., “Designing and Modeling of Efficient Resonant Photo Acoustic Sensors for Spectroscopic Applications,” J. Mod. Phys., 2 (4) (2011) 200–209.

Yehya F. & Chaudhary A. K., Konda S. & Rasel A A “Time Resolved Pulsed Photoacoustic Spectroscopy of Formaldehyde Molecules at 266 nm” Albaydha University Journal (BUJ)- vol(2)– Issue 3(2020) 186-19